# A New Method of InSAR Phase Unwrapping Processing Considering the Terrain Factors

**J G Liu[1], J F Wang[1], Z L Wang[1] and W K Liu[2,*]**

[1]Power Supply Ltd of Tai an, Shandong, 8 Dongyue street, Taishan district, Taian city, Shandong province China
[2]Center of information, Shandong University of Science and Technology, 579 Qianwangang Road, Qingdao, China

Corresponding author and e-mail: W K Liu, weike.liu@163.com

**Abstract.** Interferometric synthetic aperture radar interferometry (InSAR) phase unwrapping is influenced by the terrain factors, how to consider the terrain factors especially the complex ones is meaningful to the unwrapping algorithm. In order to solve this problem, based on the terrain phase statistical information, this paper proposes a phase gradient estimation(PGE) model applied for the additional constraint condition to the nonlinear least squares phase unwrapping. It involves the model not only eliminates noise influence, but also considers the terrain factors. Finally, real data unwrapping experimental results, comparing the proposed algorithm with classical approaches, illustrates the effectiveness the PGE phase unwrapping algorithm could be used to eliminate the effect of topography variation in the unwrapping process.

## 1. Introduction

Interferometric synthetic aperture radar (InSAR) phase unwrapping is one of the most important steps to obtain the DEM and minor deformation of topography[1], but it is also influenced by the topography factors, which is the main source of errors for InSAR products.

Currently typical phase unwrapping methods are based on the optimal estimate, such as weighted method [2], instantaneous frequency (IF) estimation method [3], nonlinear Kalman filter method [4], nonlinear phase model algorithm [5] and ant colony optimization algorithm [6] and so on. Typical algorithms are based on the assumptions: the topography is continuously changing, but the main interferometric phase values are discontinuous, the growth of ground range sampling rate and baseline de-coherence lead to the actual phase unwrapping errors. Therefore, taking into account the topography factors to the phase unwrapping, it could be effective to introduce the topography-related input control variables in phase unwrapping models. There are three ways to take into account the terrain factors: 1) using the interferometric phase spectrum shift, which is closely related to the angle of terrain slope [7]; 2) using the linear phase of the interferometric phase to estimate the slope of the topography [8]; 3) using the obtained DEM of the region from optical or US space mission SRTM.

In this paper, based on the topography statistical information, the phase gradient estimation (PGE) model is proposed as the constraint condition of the nonlinear least squares phase unwrapping algorithm. Finally, the unwrapping experimental results show that this algorithm is accurate and

robust. The algorithm could effectively take into account the topography factors and restrains the errors propagation.

## 2. PGE model

Suppose the slope angle is $\tau$ in the SAR interferogram. In the vertical (perpendicular to the orbit) and azimuth (parallel to the orbit) direction, the average angles are $\tau_y$ and $\tau_x$. The slant distance of the two points is the (1):

$$\Delta R = R_1 - R_0 = \sqrt{(H - z_0 + B_v)^2 + (y - B_h)^2} - \sqrt{(H - z_0)^2 + y_0^2} \tag{1}$$

Then the phase difference $\Delta R$ can convert into the components sum of three directions: in line of sight (LOS), azimuth and vertical direction. The (2) shows the phase difference caused by the topography deformation which could respectively decompose in three vector directions:

$$
\begin{aligned}
\Delta\phi &= -\frac{4\pi}{\lambda} \cdot (R_0 - R_1) = \frac{4\pi}{\lambda} \cdot \left( (R_1 - R_1') + (R_1' - R_0) \right) \\
&= \frac{4\pi}{\lambda} \cdot \left[ \Delta R_1 + B\cos(\theta_1 - \alpha)(z - z_0)/(R\sin\theta) \right] \\
&= \frac{4\pi}{\lambda}
\begin{bmatrix}
\left( \dfrac{1 + \tan\theta\tan\tau_y}{2\tan\theta} \right)(R_1' - R_0) + \\[2ex]
\dfrac{B_\perp}{R_0} \dfrac{\tan\tau_x \cos\tau_y}{\sin(\theta - \tau_y)}(x - x_0) + \\[2ex]
\dfrac{B_\perp}{R_0} \dfrac{\cos\tau_y}{\sin(\theta - \tau_y)} h
\end{bmatrix}
\end{aligned}
\tag{2}
$$

Where $\theta$ is the incidence angle, and $\theta = (\theta_1 + \theta_2)/2 \approx \theta_1 \approx \theta_2$, $\theta_0 = \theta_1 - \theta_2 \approx B_\perp/R_0$, $\cos\tau_y = (y - y_0)/S'$, $\Delta R_0 = R_0' - R_0$, $\Delta R_1 = R_1 - R_1'$, $(z - z_0) = (y - y_0)\tan\tau_y \sin\tau_x + h = (x - x_0)\tan\tau_x + h$, $\sin\theta = \Delta R_1/(y - y_0) = \sin(\theta - \tau_y)/\cos\tau_y$, $S' = \Delta R_1/\sin(\theta - \tau_y)$.

Let the vector $\Delta f = [\Delta f_r \cdot \Delta f_x]^T = \frac{1}{2\pi}\left[ \dfrac{\partial\phi}{\partial R} \cdot \dfrac{\partial\phi}{\partial x} \right]^T = \frac{1}{2\pi}\left[ \dfrac{\Delta\phi}{\Delta R} \cdot \dfrac{\Delta\phi}{\Delta x} \right]^T$ represents the LOS and azimuth 2D IF. In order to obtain relationships of the IF component and the slope angle in the two directions, we project and divide the three vectors of the (2) in the three directions along the LOS and azimuth direction:

$$
\begin{cases}
\Delta f_r = \dfrac{\partial\phi}{\partial R} = \dfrac{1}{2\tan(\theta - \tau_y)} = \dfrac{1 + \tan\theta\tan\tau_y}{2(\tan\theta - \tan\tau_y)} \\[3ex]
\Delta f_x = \dfrac{\partial\phi}{\partial x} = k_B \dfrac{\tan\tau_x \cos\tau_y}{\sin(\theta - \tau_y)} = k_B \dfrac{\tan\tau_x}{\sin\theta - \cos\theta\tan\tau_y}
\end{cases}
\tag{3}
$$

Where $k_B = \dfrac{4\pi B_\perp}{\lambda R_0}$. The (3) has the same results as in reference [3]. Suppose the slope gradient vector is $d = [\tan\tau_y \ \tan\tau_x]^T = [d_y \ d_x]^T$, which is also the IF's function in azimuth and range direction (4):

$$\begin{cases} d_x(\Delta f_x, W) = \Delta f_x W \\ d_y(\Delta f_r) = (2\Delta f_r \tan\theta - 1)/(2\Delta f_r + \tan\theta) \end{cases} \quad (4)$$

Where $W = \cos\theta(\tan\theta - d_y)/k_B$. When the angle of topography range slope tends to $\theta$, the number of fringe wave is increasing. It was shown in the reference [7] that the probability density function (PDF) of topography slope gradient was log-normal distributed in different topography conditions. In the discrete InSAR interference image, hypothesis the slope gradient azimuth and range component are independent and distributed identically. The 2D slope gradient PDF formula is (5):

$$\begin{cases} F_d(d_x) = \sum_K \log L_{d_x} / (\pi|d|\cos\tau_x) \\ F_d(d_y) = \sum_K \log L_{d_y} / (\pi|d|\cos\tau_y) \end{cases} \quad (5)$$

Where $K$ is the size of phase estimation window, $\log L_{d_x}$ and $\log L_{d_y}$ are Log-Levy distribution of the gradient components. According to the (5) and the relationship between the IF (3) and topography slope (4), we get the IF-PDF function (6):

$$\begin{cases} func(\Delta f_r) = k \cdot \rho \Delta f_r F_d(d_y) \\ func(\Delta f_x) = k \cdot \rho \Delta f_x F_d(d_x) \\ \rho = |\cos\tau_y / \sin(\theta - \tau_y)| \\ \quad = |\cos(\arctan d_y)/\sin(\theta - \arctan d_y)| \end{cases} \quad (6)$$

Where $k$ is the proportionality constant, $\rho$ is the phase sampling rate in azimuth and range direction. According to the above transformation between the phase gradient and IF which is described in (3), the range PGE model function is (7):

$$P_{\Delta\phi_y}(\Delta\phi_y) = func\left(\frac{1}{2\pi} \cdot \frac{\Delta\phi_y}{\Delta y}\right)\frac{1}{2\pi\Delta y} \quad (7)$$

The azimuth PGE model function is (8):

$$P_{\Delta\phi_x}(\Delta\phi_x) = func\left(\frac{1}{2\pi} \cdot \frac{\Delta\phi_x}{\Delta x}\right)\frac{1}{2\pi\Delta x} \quad (8)$$

The (7) and (8) show that the PG can be obtained by the IF-PDF model. The changing trend and the residual of the phase gradient could be deduced from the PG estimation (PGE) function.

## 3. PGE Experiments

The primary parameters of the simulation experiments are shown in the Table 1.

**Table 1.** Seleted parameters of image experiment data.

| Baseline Distance(m) | Image Range($m^2$) | Ratio (m) | Satellite incidence($^\circ$) | satellite altitude (km) | radar wavelength (m) |
|---|---|---|---|---|---|
| 200 | $41\times41$ | 27 | 19 | 785 | 0.057 |

In the simulation interferogram (see Figure1) is obviously divided into two parts, the blue one is the body of water, the rest is mountain and the highest part is 300 meters high. Assuming $SNR = 0 db$ the simulation uses the PG estimation function
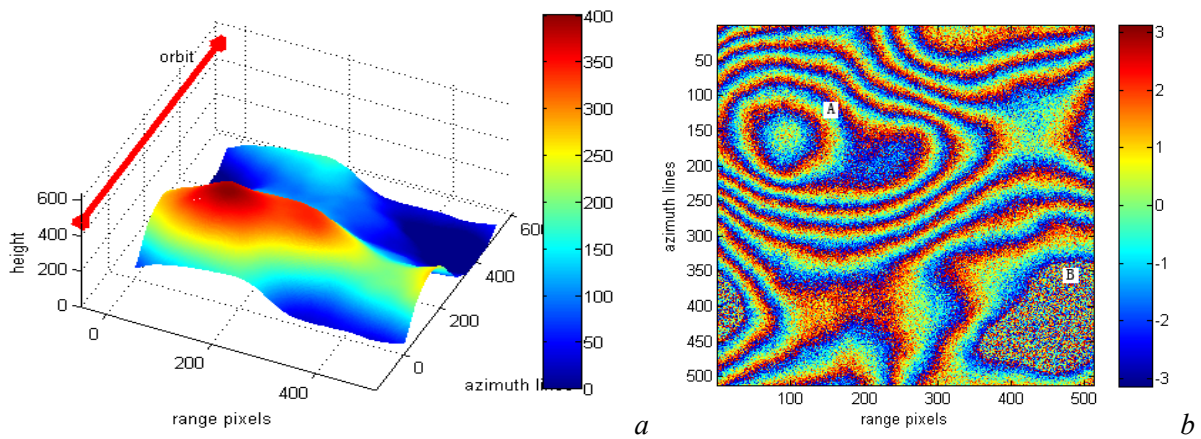
**Figure 1.** interferogram simulation(a) 3D interferogram, (b) Wrapped phase interferogram.

Parts A and B are the two obvious representative regions (see Figure 1(b)). A represents the mountains, B represents the water regions where there is the pure noise in the interferogram.
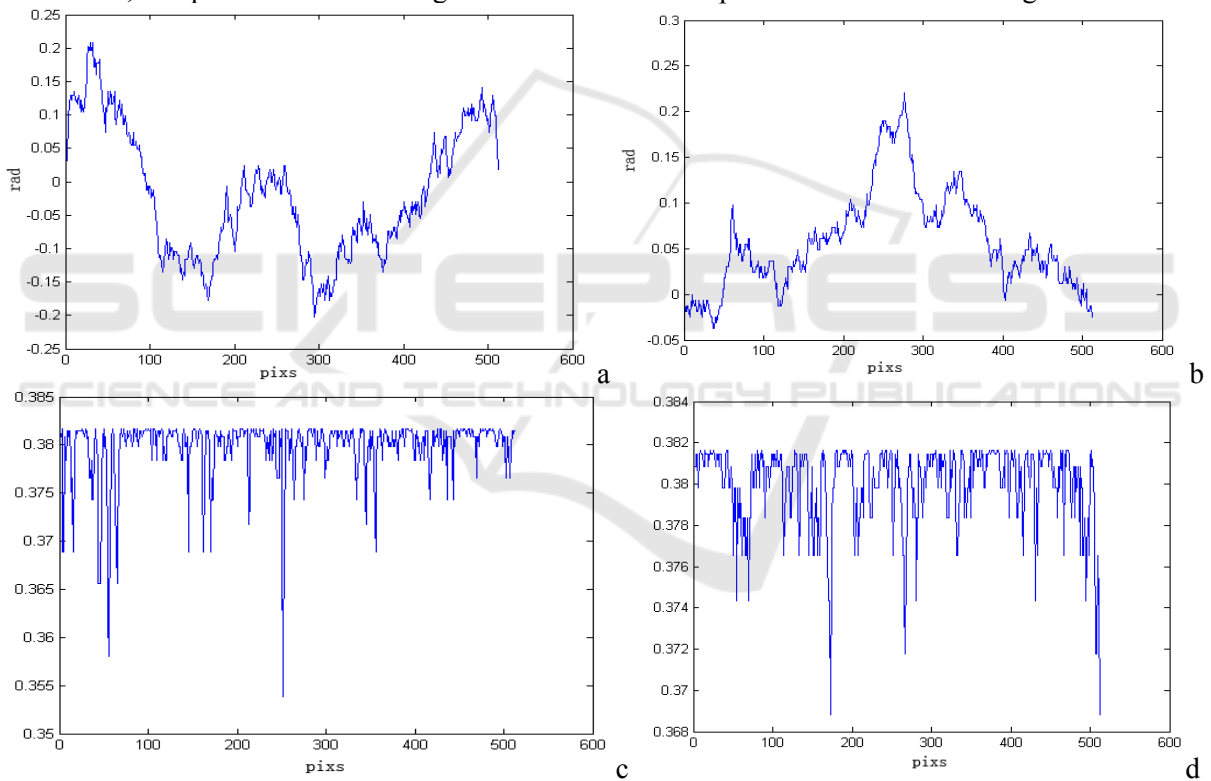


**Figure 2.** The comparison of IF estimation with PGE model of the 150 line.
(a)IF estimation in the azimuth direction; (b) IF estimation in the range direction;(c) PGE model in the azimuth direction; (d) PGE model in the range direction.
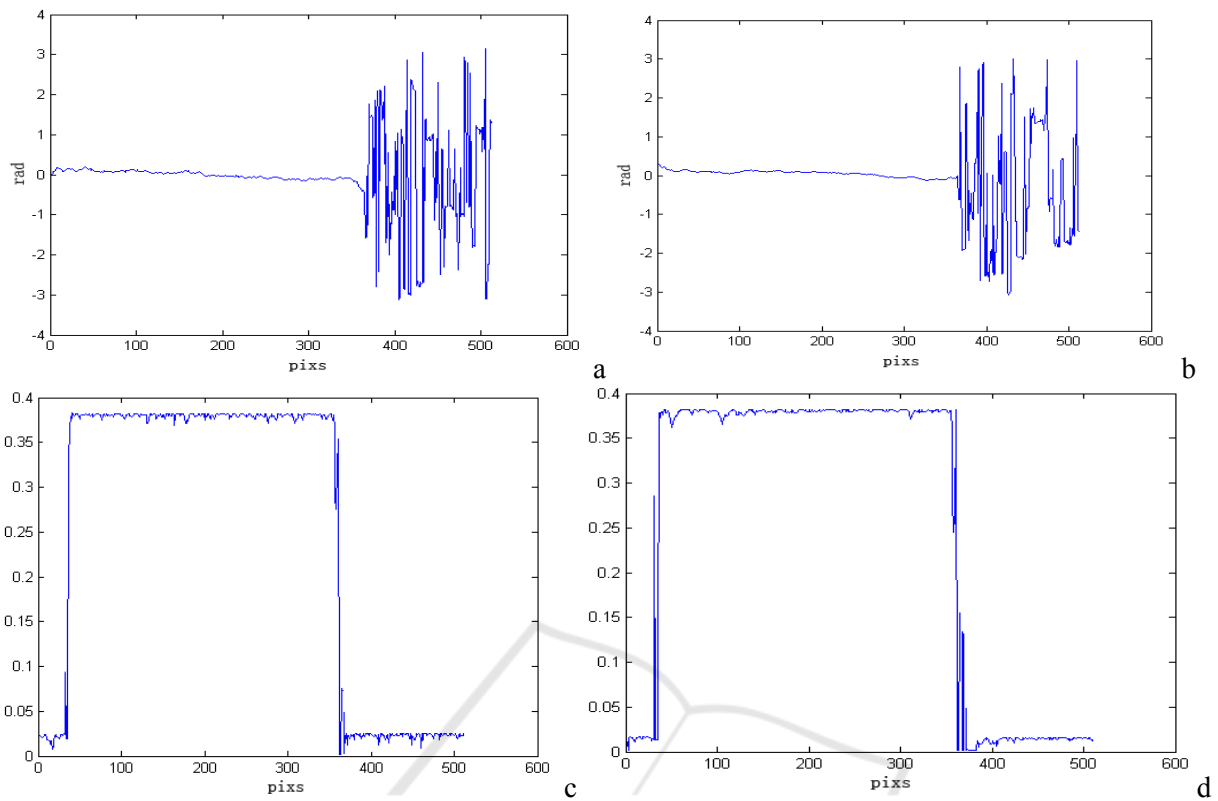
**Figure 3.** The comparison of IF estimation with PGE model of the 450 line.
(a)IF estimation in the azimuth direction; (b) IF estimation in the range direction;(c) PGE model in the azimuth direction; (d) PGE model in the range direction.

Figure 2 and Figure 3 make comparisons of the IF estimation and PGE model after the transformation of the 150 row and the 450 row of the cross section. It can be seen from Figure2 (a) and Figure2 (b), even in similar topography parts of the interferogram, the frequency still change greatly relative to the PGE model in Figure 2(c) and Figure 2(d).

In Figure 3 (a) and Figure 3 (b), the shadow region caused by the water regions, the IF estimation cannot reflected the changes, but for Figure 3 (c) and Figure 3 (d), the PGE model in the shadow areas, values are close to 0, so it reflects more accurately, that also means the it is more stable than the frequency in steep topography and shadow regions. Not same with the azimuth, the PGE in the range direction depends on the slope along the track direction and perpendicular to the track direction, which is the same as formula (4). By calculating the known region of interference, the superiority of PGE parameter model could able to estimate and infer the phase gradient in distortion regions, which could get the more accurate estimates.

## 4. Phase unwrapping model and Unwrapping experiments

The topography slope derivation formula (3) shows that the trend of topography variation is nonlinear [9]. Using the additional constraints of the PGE model to pre-estimate phase gradient, the least squares phase unwrapping algorithm is taking into account the nonlinear variation of the topography slope. The nonlinear least squares phase unwrapping with PGE constrain is as (9):

$$\min L(\phi) = \left\| \Delta\phi_y - 2\pi f_y \right\|^2 + \left\| \Delta\phi_x - 2\pi f_x \right\|^2$$
$$s.t. \ \ [P_{\Delta\psi|x,y}(\bar{\psi}^t|x,y) - P_{\Delta\psi|x,y}(\bar{\psi}^{t-1}|x,y)] < \xi \tag{9}$$

676

This unwrapping model represents the minimizing deviation of all unwrapped phase frequency with the wrapped one. And the constraint ensures that the twice iteration difference of the phase gradient values is tending to zero. The model function (9) is the non-linear constraint formula due to the constraint is non-linear.

Generally, there are two ways to solve nonlinear equations, one is to use the prior knowledge to determine the initial value to reduce the amount of calculation, and then use the quadratic programming methods or techniques based on the global trust-region strategy. In addition, the constrained optimization problem can be transformed into the non-constrained optimization problem [10]. In order to test and verify the effectiveness of the PGE unwrapping algorithm, the experiment uses two CEOS scenes of the ALOS satellites in the Middle East from July 24, 2007 and September 8, 2007. Interferometric regions have large terrain undulation and rich details.

The Figure 4 shows the original cutting interferogram corresponding image block size is 1024 * 1024 pixels. The experiment compares the algorithms of LS, WLS and Snaphu[11] (classic minimal network flow unwrapping algorithms) with PGE phase unwrapping algorithm. The unit is pixel in Figure 4.
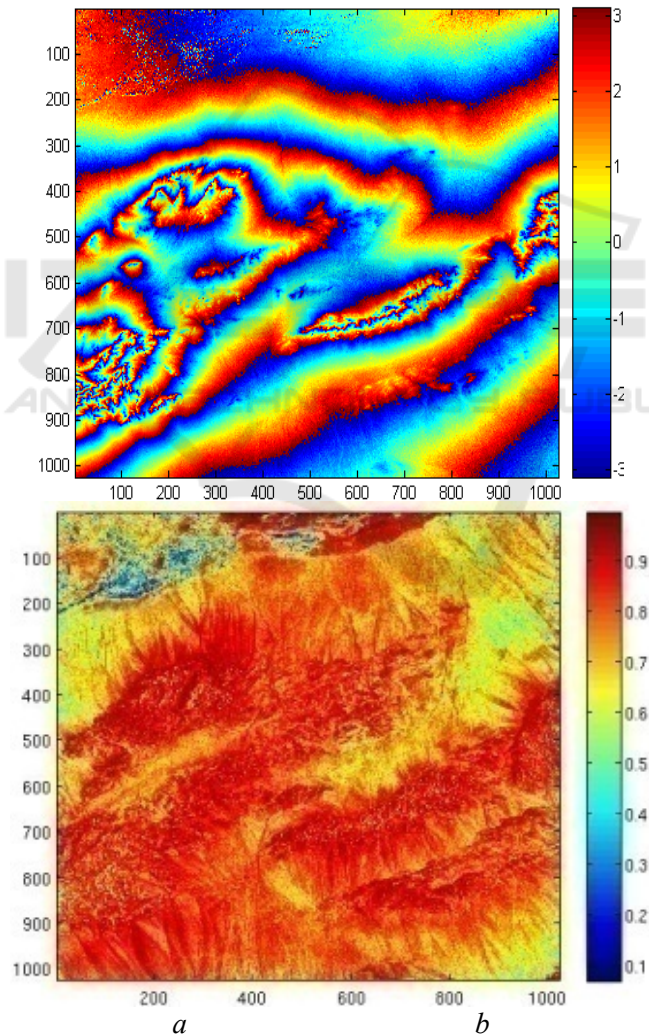


**Figure 4.** Original and coherence of the Middle East ALOS satellite interferogram. (a)original interferogram, (b) coherent.

The result of original phase interferogram of 4(a) and coherent of 4(b) shows that the highlight of the regional coherence is well, dark spots regional coherence is poor. The relationship between the topography experimental regions with its expanded the phase is $H(x,y) = \lambda\phi(x,y)/4\pi$, that formula can be used inverting landscape and get the three-dimensional surface topography [12], as is shown in Figure 5.
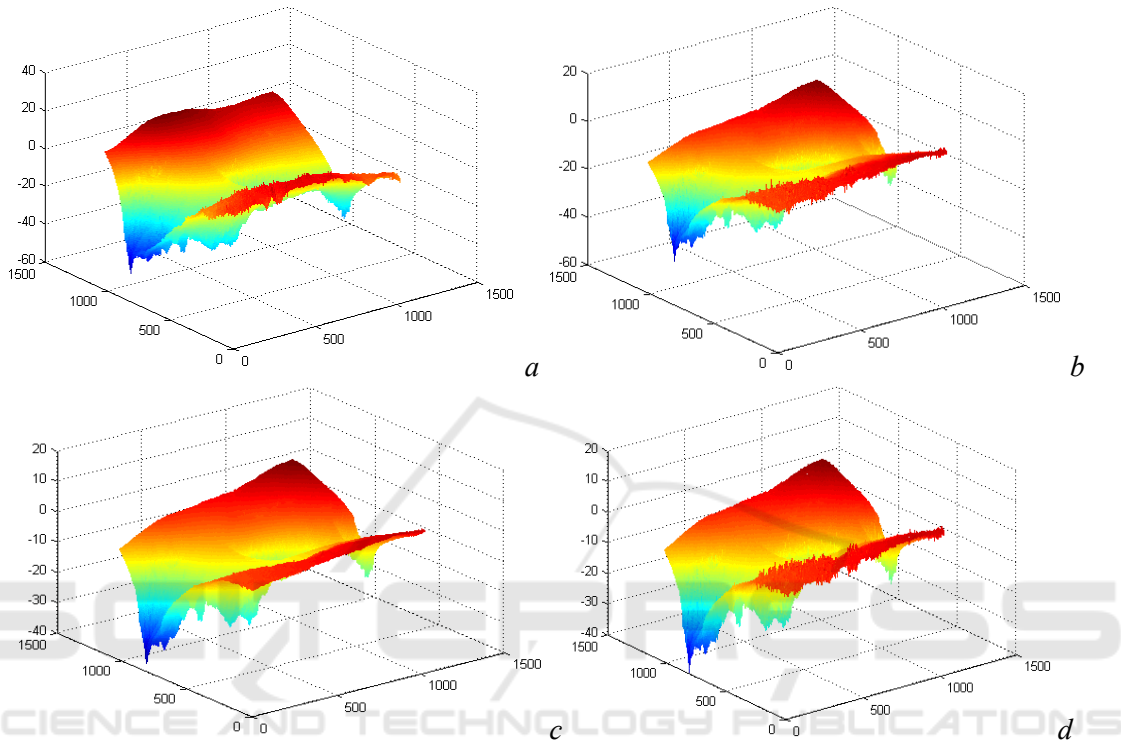


**Figure 5.** 3D phase unwrapping images (a)LS Phase unwrapping, (b) WLS Phase unwrapping, (c) Snaphu Phase unwrapping, (d) PGE Phase unwrapping.

The unwrapped 3D Figure 5(a~d) reflect that LS phase unwrapping result is the smoothest result even under the different topography conditions, but it also caused the global transmission of errors, the unwrapped phase values range from -60 to 40. Relative to the LS algorithm, WLS and Snaphu phase unwrapping methods are better reflect the quality of the different topography areas, but it could not distinguish different kinds of phase information, the unwrapped phase values range from -60 to 20 and -40 to 20. For the two algorithms does not consider the influence of topography factors, the regional unwrapped results is deviated from the actual existence of the topography changes, especially in the regions where topography changes abruptly. The PGE algorithm reflects the more detailed than the optimization algorithms, which proves the method can reduce the effect of phase residuals caused by the topography factors. The unwrapped phase values range between -40 to 20, it takes into account the topography factors of geometric distortion effects on unwrapping. Compared with the other algorithms, it has a higher accuracy.

Table 2 compares a set of quantitative indicators to analyse the comparative merits of different unwrapping algorithms.

**Table 2.** Unwrapped time, RMSE and $\varepsilon$ values.

| Algorithm | Run Time(s) | RMSE (rad) | $\varepsilon$ value(rad) |
|-----------|-------------|------------|--------------------------|
| LS | 93.69 | 10.7148 | 0.7763 |
| WLS | 198.98 | 3. 9802 | 0.5628 |
| Snaphu | 977.32 | 3. 3841 | 0.5269 |
| PGE | 638.73 | 2.0867 | 0.3269 |

The results are running in Matlab2008 environment Ubantu operating system
(Computer CPU is Intel (R) Pentium (R) 3.20GHz, memory is 2G).

It can be seen that the LS unwrapping algorithm has the least computation time. But compared with the other quotas, Snaphu algorithm has the most running time. The reason is that finding the minimum network flow takes more time on the large interferogram and but the number of phase residuals is the largest. The running time of PGE unwrapping method is less than Snaphu but longer than LS. It takes 192.630s to solve the frequency conversion, which was also added to the phase unwrapping time. But the PGE has the best results in the rest of quotas: RMSE and the $\varepsilon$ value. It also shows that PGE algorithm is stability and adaptability that can get relatively reliable unwrapping results. And the results provide a perfect fit to the phase gradient estimated based approach, which is the probability of a biased estimate (shaded part) because of the topography to reduce the number of generated residual handicap.

From all quotas, PGE unwrapping algorithm has more accuracy and adaptability to the method regardless of topography factors. Based on the PG estimation model can estimate, optimize phase gradient and guide LS optimization phase unwrapping. In the case of increasing the amount of limited computing to take into account the topography factors, the approach has increased the ability to resist the phase distortion.

## 5. Conclusions

The same InSAR interferogram has the same baseline, but different topography caused different slant range, and then caused the different PG. In other words, different PG means different topography information in the interferogram. In the local region, estimated PG reflects the changing trend of the phase and the probability of the different PG falls in the corresponding interval. From the above derived formulas, the phase IF is consistent with the variation of slope angle and the PG. Based on the principle of Woodward [13, 14], by separately calculating the range and azimuth phase IF, the statistical characteristics of PG could estimate the phase in different topography conditions, so the PGE model can take into account the changes of topography factors and be applied into the phase unwrapping as the constraint condition. The experiment shows unwrapped phases have more accurate results than some typical phase unwrapping algorithms.

## Acknowledgement

## References

[1]    Zhong H, Tian Z and Huang P 2015 A combined phase unwrapping algorithm for InSAR interferogram in shared memory environment *International Congress on Image & Signal Processing* pp 1504–1509
[2]    Cui H H, Liao W H and Cheng X S 2010 Mathematic Descriptions and Analysis of Quality

Weighting Factors in Phase Unwrapping Algorithms *ACTA OPRICA SINICA* vol 30 (1) pp 97–104

[3] Liang M, Zhang Z B and Zhong J G 2016 Phase unwrapping guided by instantaneous frequency for wavelet transform profilometry *Journal of Optoelectronics laser* vol 27 (8) pp 853–862

[4] Xie X M and Zeng Q N 2015 Efficient and robust phase unwrapping algorithm based on unscented Kalman filter, the strategy of quantizing paths-guided map and pixel classification strategy *Applied Optics* vol 54 (31) pp 92–94

[5] Huang H F and Wang Q S 2014 A Method of Filtering and Unwrapping SAR Interferometric Phase Based on Nonlinear Phase Model *Progress in Electromagnetics Research* vol 144 (1) pp 67–78

[6] Wei Z Q, Xu F and Jin Y Q 2008 Phase unwrapping for SAR interferometry based on an ant colony optimization algorithm *International Journal of Remote Sensing* vol 29 (3) pp 711–725

[7] Guarnieri A M 2003 Using topography statistics to help phase unwrapping *IEEE Proceedings Radar Sonar Navigation* vol 150 (3) pp 144–151

[8] Zhu D Y and Zhu Z D 2005 Improving the Coherence for InSAR Processing and Coherence Estimation Using the Linear Phase Model *ACTA ELECTRONICA SINICA* vol 33 (9) pp 1594–1598

[9] Wang Z Y, Zhang J X and Huang G M 2014 Precise monitoring and analysis of the land subsidence in Jining coal mining area based on InSAR technique *Journal of China University of Mining & Technology* vol 43 (1) pp 169–174

[10] Liu W K, Liu G L and Tao Q X 2012 Nonlinear least squares phase unwrapping based on homotopy method *Science of Surveying and Mapping* vol 37 (4) pp 126–128

[11] Syakrani N, Baskoro E T and Mengko T L 2015 New weighting alternatives to MCFN phase unwrapping', *International Journal of Tomography & Simulation* vol 28(3) pp 39–52

[12] Liu G L, Hao H D and Tao Q X 2009 The Implementation and Analysis of Kalman Filter Phase Unwrapping Algorithm of InSAR *International Conference on Geo-spatial Solutions for Emergency Management (GSEM) and 50th Anniversary of Founding of Chinese Academy of Surveying and Mapping* XXXVIII pp30–34

[13] Boyd J P 2015 Convergence and error theorems for Hermite function pseudo-RBFs: Interpolation on a finite interval by Gaussian-localized polynomials *Applied Numerical Mathematics* vol 87 pp 125–144

[14] Chen C W and Zebker H A 2002 Phase unwrapping for large SAR interferograms: statistical segmentation and generalized network models *IEEE Trans on Geosci Remote Sensing* vol 40 (8) pp1709–1719